Improved Analysis for Flexural Creep with Application to Sialon Ceramics

Ching-Fong Chen*,*

Department of Materials Science and Engineering, The University of Michigan,
Ann Arbor, Michigan 48109

Tze-jer Chuang*

Ceramics Division, National Institute of Standards and Technology, Gaithersburg, Maryland 20899

By using a statistical least-squares method to minimize the differences between predicted and measured load-point displacement rates from four-point bend specimens, power-law creep parameters for tension and compression were estimated. An alternative but simpler method of estimating power-law creep parameters from flexural creep data is also proposed. This method entails the direct measurements of steady-state creep strain rates at two stress levels by an indentation technique. Based on a closed-form solution, the power-law creep parameters could then be estimated from both the measured neutral axis locations and curvature rates. The results from these two methods compare favorably with one another, and with the simple compressive creep data. Both methods yield a high stress exponent of about 14 for tension and a stress exponent of about unity for compression. Cavitation-enhanced creep in tension and diffusional creep in compression are responsible for this asymmetric behavior. [Key words: sialons, flexure, creep, tensile, compression.]

I. Introduction

AT STEADY STATE, the thermal creep of ceramics under sustained loading conditions normally exhibits a power-law stress-dependent behavior.[1] Typically, flexural creep tests are used to investigate this type of behavior. Flexural creep tests offer several advantages such as (1) ease in aligning and fixturing and (2) economics in specimen preparation and facility construction.

Hollenberg et al.[2] presented the first analysis in which stresses and strains in crept beam specimens could be calculated from bend test data, provided that the tensile creep behavior is identical to its compressive counterpart, and as a result, the neutral axis is located at the geometric center. Despite the wide use of this analysis as a general means of creep behavior characterization, the results could be incorrect because of these unrealistic assumptions. At elevated temperatures, damage in the form of boundary cracks and cavities occurs in the tensile side of a bend specimen for a large number of two-phase ceramics.[3–9] This, coupled with the fact that ceramics normally creep faster in tension than in compression,[10–15] results in an asymmetrical stress distribution

and a shift of the neutral axis in a bend-beam specimen during creep.

A more generalized approach was developed by Chuang,[16] who postulated independent power-law relations in tension and compression. In his analysis both the power-law creep preexponent and the exponent are independent variables.

In the present investigation, Chuang's method is used for the creep characterization of an annealed sialon–YAG ceramic. In order to increase the accuracy of the estimation of power-law creep parameters, this paper uses a statistical least-squares method to minimize the errors between experimental data and predicted load-point displacement rates. Hence, uniaxial power-law parameters for both tension and compression could be obtained from the flexure data more accurately.[17] To enhance the degree of confidence in this estimation, the locations of neutral axes were measured as a function of stress and checked against predictions based on estimated creep parameters.

The estimation method by Chuang[16] involves dedicated computation and programming, and the implementation of this methodology in practical applications requires special expertise. In order to bypass this drawback, an alternative method is proposed in which the computer analysis can be replaced by measuring the midspan creep strains at two different stress levels using an indentation method. Closed-form solutions are provided to directly compute the creep parameters from the neutral axis locations and curvature rates measured during steady-state creep at any two stress levels. The resulting stress exponents are interpreted in terms of cavitational damage in tension and a diffusional mechanism in compression. The effect of this asymmetrical creep behavior in tension and compression on the redistribution of stress will also be discussed.

II. Experimental Procedure

(1) Sample Preparation and Flexural Test

The chemical composition of the material prepared for this study was annealed β-$Si_{6-x}Al_xO_xN_{8-x}$, where $x = 0.77$ (10 equiv% Al; 0 equiv% refers to Si_3N_4; 100 equiv% refers to AlN), containing 7 vol% of garnet ($Y_3Al_5O_{12}$). This composition is designated as β_{10}-7G, meaning β-phase with 10 equiv% Al and 7 vol% garnet. The starting materials include Si_3N_4, Al_2O_3, AlN, and yttrium acetate. Weighed powders were ball-milled in methanol for 8 h. Yttrium acetate was dissolved in methanol to ensure uniform mixing. Slurries were dried at 80°C for 5 h and then 110°C for 16 h. Since yttrium acetate decomposes at ≈390°C, calcination was conducted at 400°C for 24 h in air. These samples were hot-pressed under a pressure of 20 MPa in a mild flow of nitrogen gas at 1750°C for 60 min followed by annealing at 1250°C for 50 h. Specimens in dimensions of 2.1 mm × 2.8 mm × 35 mm with longitudinal marks and chamfered corners were

machined from hot-pressed billets in such a way that the tensile surfaces were parallel to the hot-pressing direction. Only samples with a weight loss of 2 wt% or less after hot-pressing were chosen for actual testing.

Experiments were conducted using four-point bending as a test technique. The inner loading points were spaced at 5 mm whereas the outer span at 20 mm. The inner load-point deflections were monitored by an external linear variable differential transducer (LVDT). The accuracy of the measurements is within ± 2 μm.

(2) Neutral Axis Measurement

This method is similar to the technique that was originally used by Wiederhorn *et al.*[18] A schematic of the method used for the neutral axis measurement is shown in Fig. 1. Prior to creep testing, two straight rows of Vickers indentation marks were placed at a distance, $L_0 = 2.0$ mm, apart within the inner span on a side surface of the specimen that had been polished to a 0.1-μm finish. Care was taken to ensure that the indentations were large enough to be visible during postcreep examination but not large enough to influence the creep behavior.[19,20] It appeared that an 8-N indentation load was appropriate for sialon ceramics. As steady-state creep was reached, the tests were interrupted. The distances, L, between the two rows of indentations were measured and the corresponding strains calculated as $\epsilon = (L - L_0)/L_0$.

(3) Compressive Creep Test

The specimens used in creep testing were machined to 2.1 mm $\times$ 2.8 mm $\times$ 7.0 mm with longitudinal machining marks and chamfered corners. Compressive creep tests were conducted in an Instron testing machine in a dead-weight loading mode. To measure the compressive strain on the specimen, the following procedures were used. Two silicon carbide pedestals 5 mm $\times$ 5 mm $\times$ 3 mm were placed on the top and the bottom of the specimen (Fig. 2). Using a remote telescope with an accuracy of 1 μm, the separation between the edges of these pedestals was monitored, and from this the strain could be calculated. Load was transmitted to the pedestals and the specimen by means of two silicon carbide blocks that were 12 mm $\times$ 12 mm $\times$ 12 mm. These blocks were inserted between the silicon carbide rams attached to
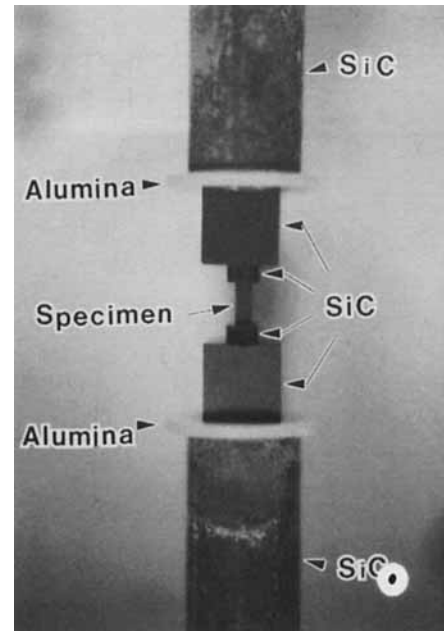

Fig. 2. Experimental setup for the compressive test. Two alumina disks were placed between the silicon carbide pushing rods and the siliconized silicon carbide to avoid sticking.

the crosshead of the testing machine (Fig. 2). Since the blocks had larger areas of cross section than the specimen, they served to prevent formation of high stresses at the point of contact area between the specimen and the rams. Two disks of alumina, 26 mm in diameter and 3 mm thick, were placed between the load-transmitting blocks and the rams (in order to prevent sticking due to reaction between the two materials at the high test temperatures.) After the furnace was heated to the designated test temperature and stabilized for approximately 1/2 h, the load was applied.

III. Results and Discussion

(1) Estimating Power-Law Creep Parameters by Numerical Method

In this section, a generalized approach developed by Chuang[16] will be applied. This model postulated independent power-law relations in tension and compression where both the power-law creep preexponent, A, and the exponent, n, are independent variables. A further modification of Chuang's analysis will be made to apply a statistical least-squares method to minimize the errors between experimental data and predicted load-point displacement rates. In this way, the uniaxial power-law parameters for both tension and compression could then be obtained from the flexure data with higher accuracy.[17]

(A) Theoretical Analysis: For most ceramics, the steady-state strain rate and the applied stress can be related by the power-law creep equations:[1]

$$\dot\epsilon_s = A_c(\sigma/\sigma_0)^{n_c} \qquad (\sigma, \dot\epsilon_s \text{ in compression}) \qquad (1a)$$

$$\dot\epsilon_s = A_t(\sigma/\sigma_0)^{n_t} \qquad (\sigma, \dot\epsilon_s \text{ in tension}) \qquad (1b)$$

where A and n are creep constants, and σ_0 is a normalization constant which has the same unit as stress.

Assuming that planar sections remain planar during bending, the strain ϵ of an element is linearly dependent on the distance Y from the neutral axis; namely, $\epsilon = KY$ where the curvature K serves as a proportionality constant (Fig. 3). Thus, the strain rate of a beam element is reduced to $\dot\epsilon = \dot K Y + K \dot Y$. The second term is generally negligible because during steady state, the neutral axis migration rate is very
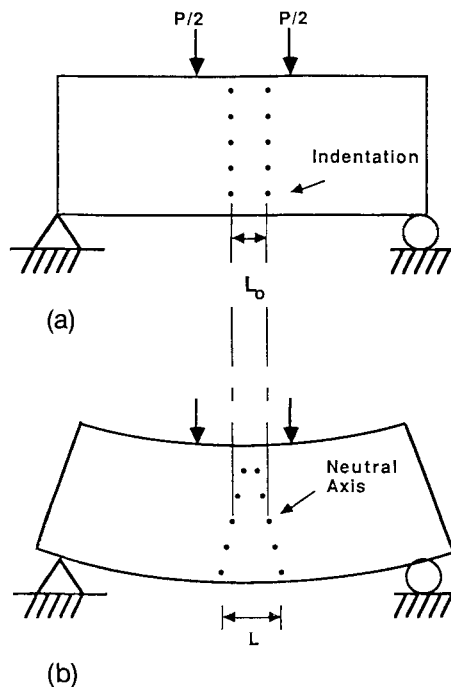

Fig. 1. Schematic showing the neutral strain axis measurement by indentation techniques: (a) before creep, (b) after creep.
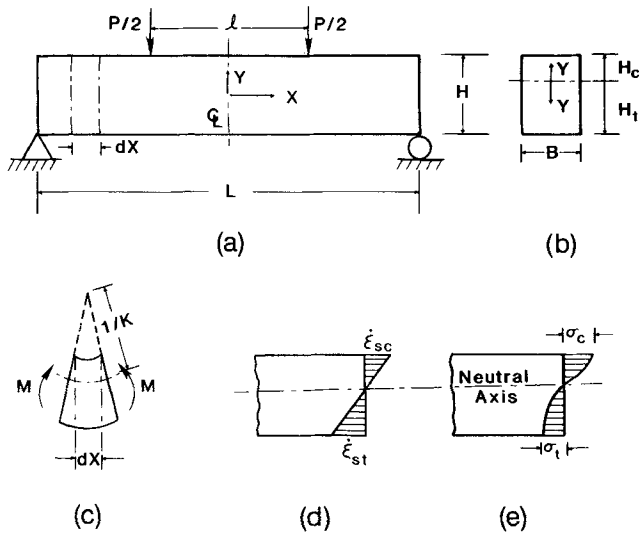
Fig. 3. Schematic showing a four-point bend beam: (a) loading configuration, (b) representative cross section, (c) typical element of deformed shape, (d) strain-rate distribution, and (e) stress distribution.

small. Thus Eqs. (1a) and (1b) become

$$\sigma = \sigma_0\left(\frac{Y\dot{K}}{A}\right)^{1/n} = \sigma_0\left(\frac{y\dot{k}}{A}\right)^{1/n} \qquad (2)$$

where $y = Y/H$, $\dot{k} = \dot{K}H$, and H is the beam height (Fig. 3). Equation (2) is valid for both stresses in compression and in tension. The equilibrium requirement dictates that the total force acting on the compressive side of the cross section be counterbalanced by its tensile counterpart. After some mathematical manipulations of Eqs. (1) and (2), this force balance equation finally reduces to

$$\left\{\frac{A_t^{1/(n_t+1)}}{A_c^{n_t/n_c(n_t+1)}}\dot{k}^{(n_t-n_c)/n_c(n_t+1)}\left[\frac{n_c(n_t+1)}{n_t(n_c+1)}\right]^{n_t/(n_t+1)}\right\}h_c^{n_t(n_c+1)/n_c(n_t+1)}$$

$$+ \; h_c = 1 \qquad (3)$$

where $h_c = H_c/H$ is a dimensionless parameter. H_c is the distance between the compressive surface and the neutral axes (Fig. 3). Equation (3) is a nonlinear algebraic equation which can be used to predict the location of the neutral axis within the inner span of a crept beam.

In addition, the requirement that the summation of moments produced by local tractions be equated to the external moment M forms the second governing equation:

$$m = \dot{k}^{1/n_c}\left[A_t^{-1/n_t}\dot{k}^{(1/n_t-1/n_c)}\frac{n_t}{2n_t+1}(1-h_c)^{(2n_t+1)/n_t}\right.$$

$$\left.+ \; A_c^{-1/n_c}\frac{n_c}{2n_c+1}h_c^{(2n_c+1)/n_c}\right] \qquad (4)$$

where $m = M/(BH^2\sigma_0)$ is the normalized applied moment and B is the width of the beam. Equations (3) and (4) constitute a system of algebraic equations for the two unknowns h_c and $\dot{k}$.

For a given material with a well-defined relationship between $\dot{k}$ and m, the load-point displacement rate incurred from a four-point beam can be solved numerically by the integration of $\dot{k}$ along the beam length x, with a linear moment distribution in the outer span and a constant maximum moment in the inner span. The differential equation to be solved is then $d^2\dot{y}/dx^2 = \dot{k}(x) = f(m)$ with $\dot{k} = f(m)$ as given in Eq. (4). Setting the origin of the coordinate system at the midspan of the deformed beam, the proper boundary conditions are $\dot{y}(0) = 0$ and $\dot{y}'(0) = 0$ due to symmetry. After the deformed shapes $\dot{y} = \dot{y}(x)$ are solved, the load-point displacement

rate is given by $\dot{\Delta}_p = \dot{\Delta}(L/2) - \dot{\Delta}(\ell/2)$ where L and ℓ are the lengths of the major and minor spans, respectively.

Once these two one-dimensional arrays (applied moment and load-point displacement rate) are determined, a least-squares subroutine will be used to fit the numerical results and experimental data. After a series of least-square iterations, a theoretical estimation of the power-law creep parameters can be obtained when those data points are well-fitted to the theoretical curve.[17]

(B) Experimental and Numerical Results: Several different creep loads were applied to annealed β_{10}-7G samples at 1170°C. An apparent steady-state creep rate was observed in all cases. After the data were collected, four reasonable power-law creep parameters were arbitrarily chosen in initial numerical calculations to generate theoretical displacement rate values. After a series of least-squares iterations, solutions of $n_c = 0.8$, $n_t = 13.8$, $A_c = 1.3 \times 10^{-10}$ s^{-1}, and $A_t = 3.5 \times 10^{-32}$ s^{-1} were obtained. The theoretical displacement rate values and experimental results are shown in Fig. 4. From these results the tensile creep behavior can be described by

$$\dot{\epsilon}_s = 3.5 \times 10^{-32}(\sigma)^{13.8} \qquad (\sigma, \dot{\epsilon}_s \text{ in tension})$$

and the compressive creep behavior by

$$\dot{\epsilon}_s = 1.3 \times 10^{-10}(\sigma)^{0.8} \qquad (\sigma, \dot{\epsilon}_s \text{ in compression})$$

where $\dot{\epsilon}_s$ and σ have the units of s^{-1} and MPa, respectively. This prediction strongly suggests a profound difference in creep behavior in tension and compression.

(C) Location of Neutral Axis: The indentation technique has been applied to measure the neutral axis position. Two sets of indentation marks ≈ 2 mm (L_0) apart (Fig. 5(a)) were made on one side of the specimen before creep loading. The test was interrupted at a designated time after steady state was reached. The distances between each set of indentations (L) after creep (Fig. 5(b)) were measured to determine the strain of each beam element. The indentation set which has zero strain is the neutral strain axis location. Figure 6 shows two typical results for the tests conducted at 1170°C and 133 MPa for 50 and 100 h, respectively.

The solutions for the normalized neutral axis positions and the experimental results from the indentation method are plotted as a function of stress in Fig. 7. Generally speaking, for the practical range of stress >50 MPa, as the applied stress increases, the compressive zone shrinks. The migration of the neutral axis toward the compressive side can be explained by the cavitation damage[21] on the tensile side. As the applied stress increases, the void density and cavity growth rate increase, resulting in a net decrease in the cross section of the bend beam on the tensile side. Therefore, as the applied stress increases, the tensile side has to increase in order
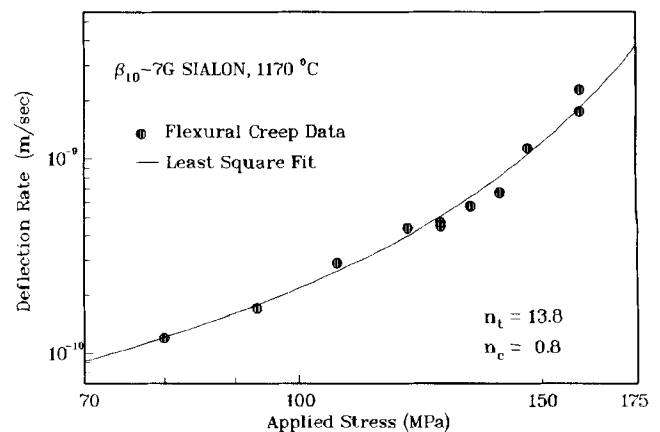

Fig. 4. Experimental results of flexural creep deflection rate vs applied stress and the numerical fitting to estimate power-law creep parameters for simple tension and simple compression creep.
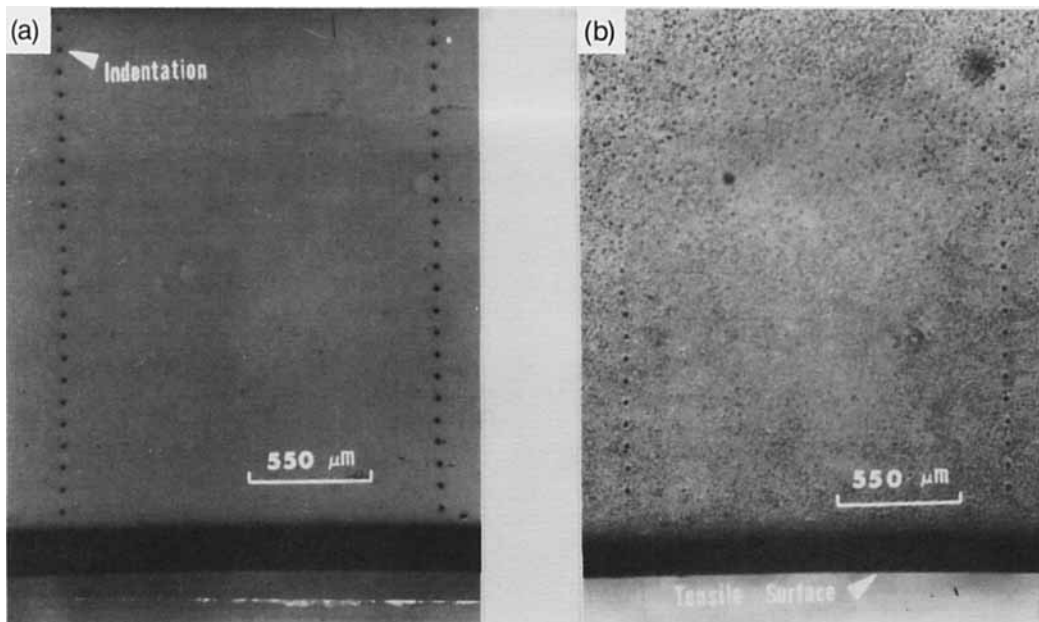
Fig. 5. Optical micrograph showing two rows of indentation marks on side of flexural specimen (a) before creep and (b) after creep at 1170°C and 120 MPa for 270 h.

to maintain the force balance. From these results, it is believed that a high n_t relative to n_c implies that the material's ability to support tensile stresses is small for a fixed creep rate. Also, a high n_t suggests that the steady-state strain rate has a very high sensitivity to the applied stress and this suggests that severe damage occurs in tensile creep.

(2) Estimating Power-Law Creep Parameters by Analytical Method

An alternative method is proposed in which the computer work can be eliminated and replaced by measuring the midspan creep strains at two different stress levels using an indentation method. Closed-form solutions will be provided to directly compute the creep parameters from the neutral axis locations and curvature rates at the two stress levels.

(A) Theoretical Analysis: Equations (1) and (2), the force balance requirements and the moment balance requirements,

form two governing equations which are described as

$$\left(\frac{\dot{k}}{A_c}\right)^{1/n_c}\left(\frac{n_c}{n_c+1}\right)h_c^{(n_c+1)/n_c} = \left(\frac{\dot{k}}{A_t}\right)^{1/n_t}\left(\frac{n_t}{n_t+1}\right)h_t^{(n_t+1)/n_t}$$

$$(5)$$

$$\left(\frac{\dot{k}}{A_c}\right)^{1/n_c}\left(\frac{n_c}{2n_c+1}\right)h_c^{(2n_c+1)/n_c} + \left(\frac{\dot{k}}{A_t}\right)^{1/n_t}\left(\frac{n_t}{2n_t+1}\right)$$

$$\times\ h_t^{(2n_t+1)/n_t} = m$$

$$(6)$$

respectively. These parameters have the same definition as previously mentioned. The parameters k, h_c, and h_t will be measured by using the indentation method; therefore, they will be treated as given. The power-law creep parameters are then determined by the following analysis. For two different
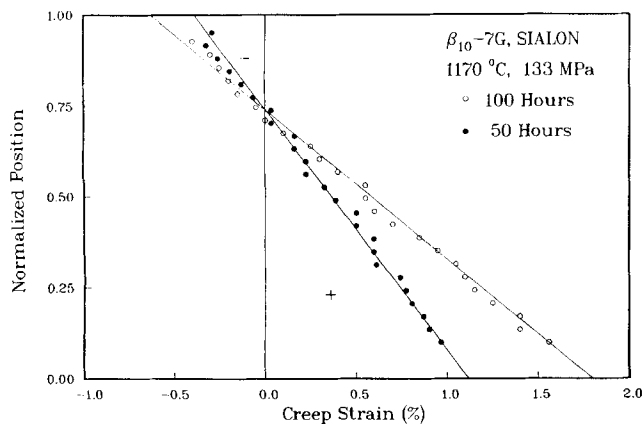

Fig. 6. Typical creep strain as a function of normalized position for creep at 1170°C and 133 MPa for 50 and 100 h: (+) tension, (−) compression.
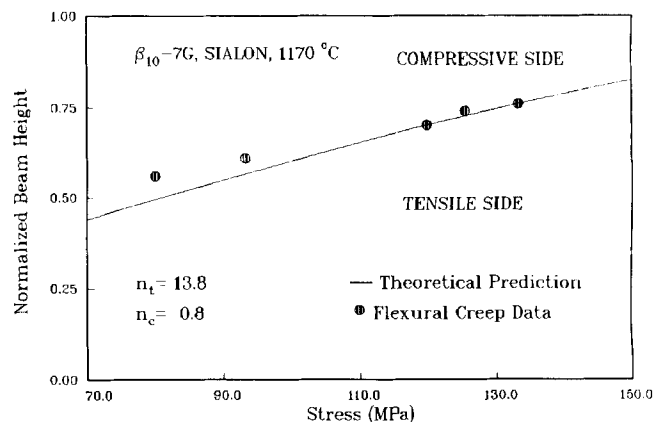

Fig. 7. Experimental neutral axis position as a function of applied stress shows a very good agreement with the theoretical prediction.

normalized applied bending moments m_1 and m_2, there are two corresponding neutral axis positions h_{c1} and h_{c2}, and two corresponding curvature rates $\dot{k}_1$ and $\dot{k}_2$. Hence, two force balance equations for these two applied stresses would be

$$\left(\frac{1}{n_c}\right)\ln \dot{k}_1 - \left(\frac{1}{n_c}\right)\ln A_c + \ln\left(\frac{n_c}{n_c+1}\right)$$
$$+ \left(\frac{n_c+1}{n_c}\right)\ln h_{c1} = \left(\frac{1}{n_t}\right)\ln \dot{k}_1 - \left(\frac{1}{n_t}\right)\ln A_t$$
$$+ \ln\left(\frac{n_t}{n_t+1}\right) + \left(\frac{n_t+1}{n_t}\right)\ln h_{t1}$$

(7a)

$$\left(\frac{1}{n_c}\right)\ln \dot{k}_2 - \left(\frac{1}{n_c}\right)\ln A_c + \ln\left(\frac{n_c}{n_c+1}\right)$$
$$+ \left(\frac{n_c+1}{n_c}\right)\ln h_{c2} = \left(\frac{1}{n_t}\right)\ln \dot{k}_2 - \left(\frac{1}{n_t}\right)\ln A_t$$
$$+ \ln\left(\frac{n_t}{n_t+1}\right) + \left(\frac{n_t+1}{n_t}\right)\ln h_{t2}$$

(7b)

respectively. Similarly, there are two moment balance equations:

$$\left(\frac{1}{n_c}\right)\ln \dot{k}_1 - \left(\frac{1}{n_c}\right)\ln A_c + \ln\left(\frac{n_c}{2n_c+1}\right)$$
$$+ \left(\frac{2n_c+1}{n_c}\right)\ln h_{c1} + \left(\frac{1}{n_t}\right)\ln \dot{k}_1 - \left(\frac{1}{n_t}\right)\ln A_t$$
$$+ \ln\left(\frac{n_t}{2n_t+1}\right) + \left(\frac{2n_t+1}{n_t}\right)\ln h_{t1} = \ln m_1$$

(8a)

$$\left(\frac{1}{n_c}\right)\ln \dot{k}_2 - \left(\frac{1}{n_c}\right)\ln A_c + \ln\left(\frac{n_c}{2n_c+1}\right)$$
$$+ \left(\frac{2n_c+1}{n_c}\right)\ln h_{c2} + \left(\frac{1}{n_t}\right)\ln \dot{k}_2 - \left(\frac{1}{n_t}\right)\ln A_t$$
$$+ \ln\left(\frac{n_t}{2n_t+1}\right) + \left(\frac{2n_t+1}{n_t}\right)\ln h_{t2} = \ln m_2$$

(8b)

Subtracting Eq. (7b) from Eq. (7a), and Eq. (8b) from Eq. (8a), respectively, the preexponential constants A_c and A_t can be eliminated from the force balance equations and the moment balance equations. The results are

$$\left(\frac{1}{n_c}\right)\ln\left(\frac{\dot{k}_1}{\dot{k}_2}\right) + \left(\frac{n_c+1}{n_c}\right)\ln\left(\frac{h_{c1}}{h_{c2}}\right) =$$
$$\left(\frac{1}{n_t}\right)\ln\left(\frac{\dot{k}_1}{\dot{k}_2}\right) + \left(\frac{n_t+1}{n_t}\right)\ln\left(\frac{h_{t1}}{h_{t2}}\right)$$

(9a)

$$\left(\frac{1}{n_c}\right)\ln\left(\frac{\dot{k}_1}{\dot{k}_2}\right) + \left(\frac{2n_c+1}{n_c}\right)\ln\left(\frac{h_{c1}}{h_{c2}}\right) = \ln\left(\frac{m_1}{m_2}\right)$$
$$- \left(\frac{1}{n_t}\right)\ln\left(\frac{\dot{k}_1}{\dot{k}_2}\right) - \left(\frac{2n_t+1}{n_t}\right)\ln\left(\frac{h_{t1}}{h_{t2}}\right)$$

(9b)

Summing Eqs. (9a) and (9b), n_t can be subtracted from the equations, leaving n_c as the only variable. Similarly, subtracting Eq. (9b) from Eq. (9a), n_c can be subtracted from the equations, leaving n_t as the only variable.

After some mathematical manipulations the power-law creep exponents for both compression and tension finally

reduce to

$$n_c = \frac{2\ln\left(\frac{\dot{k}_1 h_{c1}}{\dot{k}_2 h_{c2}}\right)}{\ln\left[\frac{m_1}{m_2}\left(\frac{h_{c2}}{h_{c1}}\right)^3\frac{h_{t2}}{h_{t1}}\right]}$$

(10)

$$n_t = \frac{2\ln\left(\frac{\dot{k}_1 h_{t1}}{\dot{k}_2 h_{t2}}\right)}{\ln\left[\frac{m_1}{m_2}\left(\frac{h_{t2}}{h_{t1}}\right)^3\frac{h_{c2}}{h_{c1}}\right]}$$

(11)

In addition, the preexponential constants A_c and A_t can be obtained by summing Eqs. (7a) and (7b) and Eqs. (8a) and (8b), respectively. The results are

$$\frac{2}{n_c}\ln(\dot{k}_1\dot{k}_2) + \frac{3n_c+2}{n_c}\ln(h_{c1}h_{c2}) + \ln(h_{t1}h_{t2})$$
$$- \frac{4}{n_c}\ln A_c + \ln\frac{n_c^4}{(n_c+1)^2(2n_c+1)^2} + \ln\frac{(n_t+1)^2}{(2n_t+1)^2} =$$
$$\ln\frac{1}{m_1m_2}$$

(12a)

$$\frac{2}{n_t}\ln(\dot{k}_1\dot{k}_2) + \frac{3n_t+2}{n_t}\ln(h_{t1}h_{t2}) + \ln(h_{c1}h_{c2})$$
$$- \frac{4}{n_t}\ln A_t + \ln\frac{n_t^4}{(n_t+1)^2(2n_t+1)^2} + \ln\frac{(n_c+1)^2}{(2n_c+1)^2} =$$
$$\ln\frac{1}{m_1m_2}$$

(12b)

After some mathematical manipulations of Eqs. (12a) and (12b), the preexponents finally reduce to

$$A_c = \left\{\frac{1}{m_1m_2}(\dot{k}_1\dot{k}_2)^{2/n_c}(h_{c1}h_{c2})^{(3n_c+2)/n_c}(h_{t1}h_{t2})\right.$$
$$\left.\times \frac{n_c^4}{(n_c+1)^2(2n_c+1)^2}\frac{(n_t+1)^2}{(2n_t+1)^2}\right\}^{n_c/4}$$

(13a)

$$A_t = \left\{\frac{1}{m_1m_2}(\dot{k}_1\dot{k}_2)^{2/n_t}(h_{t1}h_{t2})^{(3n_t+2)/n_t}(h_{c1}h_{c2})\right.$$
$$\left.\times \frac{n_t^4}{(n_t+1)^2(2n_t+1)^2}\frac{(n_c+1)^2}{(2n_c+1)^2}\right\}^{n_t/4}$$

(13b)

For the case of both h_c and h_t equal to 1/2, Eqs. (10) and (11) can be simplified to

$$n_c = \ln\left\{\left(\frac{\dot{k}_1}{\dot{k}_2}\right)^2\frac{M_2}{M_1}\right\} = n_t = N$$

(14)

This result is identical to the analysis of Hollenberg et al.,[3] when n_c equals n_t.

(B) Curvature Rate Measurement: The fundamental assumption in the previous section, that planar sections remain planar during bending, will be proved in this section. This assumption is supported by the results in Figs. 5(a), 5(b), and 6. Figure 6 shows two strain vs position curves for two indentation flexural creep tests interrupted at 50 and 100 h, respectively. These two tests are both in the steady-state regime, which can be seen from Fig. 8. In Fig. 8 the load-point deflection is plotted as a function of time for the annealed β_{10}-7G sialon at 1170°C, 133 MPa. Three identical specimens were tested to (A) failure, (B) 100 h, and (C) 50 h, respectively. Curve A illustrates that an apparent steady state is reached at times longer than 50 h. The strain of each element as a function of position for specimens B and specimen C is
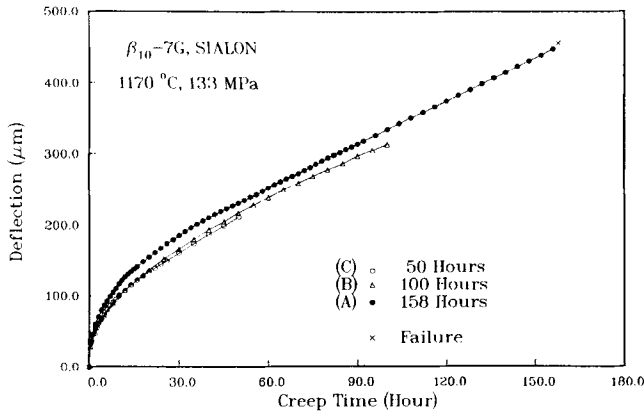
Fig. 8. Deflection as a function of creep time for three identical specimens creep at 1170°C and 133 MPa to (A) failure, (B) 100 h, and (C) 50 h. Notice that these three curves show very little sample variation.

shown in Fig. 6. The outer tensile fiber strains for these two specimens are 1.73% and 1.16%, respectively. The steady-state strain rate $\dot{\epsilon}$ is the difference between these two outer fiber strains divided by the time difference. The curvature rate can thus be obtained by the linear relationship $\dot{\epsilon} = \dot{k}y$. The results are shown in Table I. An important factor in measuring the curvature rate is that the variation in creep strain due to sample variation must be minimized. As shown in Fig. 8, there was very little difference among these three flexural creep tests due to sample variations.

(C) Analytical Results: Substituting the measured data (Table I) into Eqs. (10) and (11), one can estimate the power-law creep exponents. The resulting exponents are 0.9 for compression and 14.5 for tension. These results are very close to the estimated values from the numerical analysis. Once the stress exponents are known, both preexponents for compression and tension can be obtained from Eqs. (13a) and (13b). The resulting preexponents are $1.1 \times 10^{-10}\ \mathrm{s}^{-1}$ for compression and $8.5 \times 10^{-29}\ \mathrm{s}^{-1}$ for tension. Therefore, the tensile creep behavior can be described by

$$\dot{\epsilon}_s = 8.5 \times 10^{-29}(\sigma)^{14.5} \qquad (\sigma,\dot{\epsilon}_s \text{ in tension})$$

and the compressive creep behavior can be described by

$$\dot{\epsilon}_s = 1.1 \times 10^{-10}(\sigma)^{0.9} \qquad (\sigma,\dot{\epsilon}_s \text{ in compression})$$

where $\dot{\epsilon}_s$ and σ have the units of s^{-1} and MPa, respectively.

The predictions show very good agreement with the values that were estimated by the numerical method. A great advantage of the analytical estimation method is its simplicity. This method does not require any deflection measurements, which simplifies the experimental apparatus. Also, a simple analytical solution can be used which bypasses a lot of dedicated computation and programming. However, when choosing two applied stresses for this analytical estimation, a precaution has to be taken, namely, the experimental errors due to the sample variation. For example, if these two stresses are chosen too close to one another, the resulting estimated power-law creep behaviors probably will be covered by experimental

errors. Therefore, several recommendations can be made: (i) increase the difference in these two applied stresses; (ii) use several tests for the same load to average out the curvature rate and neutral axis position; (iii) more than two different loads can be used in order to cover nonlinear power-law creep behaviors.

(3) Stress Exponent

Values of n reported in the literature range from ≈ 1 to 14 depending on the material tested and the levels of temperature.[14,17,21-24] In view of these results, and values of n for tension and compression obtained in the present theoretical predictions are not unusual, even though they lie at the high and low ends of the range of values, respectively. Further rationalization of these results will be discussed in the following sections.

(A) Tensile Stress Exponent: A cracklike cavity mechanism had been suggested[22] which can be adopted as a primary explanation for this high tensile creep exponent. Since the rates of cavity nucleation and growth are nonlinear functions of applied stress,[4,8,25,26] it is not surprising to observe such a highly nonlinear dependence of tensile creep on the applied stress. A first-order approximation to quantify the cracking-induced creep is hereby presented. Consider a bend bar subject to load P (Fig. 9(a)) with a preexisting crack of length a (Fig. 9(b)) in the tensile side. Crack growth leads to enhancement of compliance and an energy release rate according to

$$\frac{1 - \nu^2}{E}K_I^2 = \frac{P^2}{2B}\frac{dC}{da} \qquad (15)$$

where K_I is the mode I stress intensity factor, C is the compliance of the beam, ν is Poisson's ratio, E is Young's modulus, and B is the beam width. Assuming crack growth is due to self-diffusion, a relationship between crack velocity and ap-
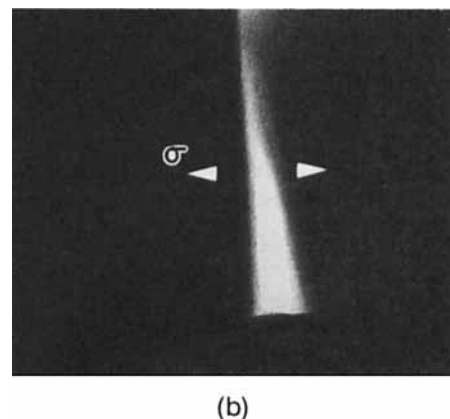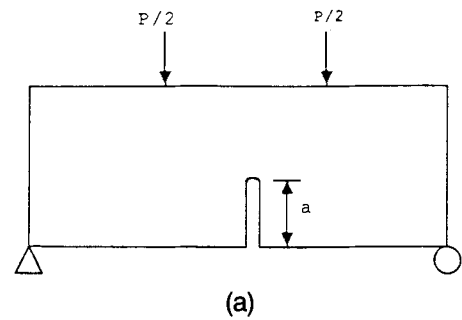

(a)

(b)

Fig. 9. Cracking-induced creep: (a) preexisting cavity of length a in the tensile side of a four-point bending bar; (b) micrograph showing the shape and the size of the preexisting cavity.

Table I. List of Normalized Neutral Axis Positions (h_c), Curvature Rates ($\dot{k}$), and Bending Moments (m) for Two Different Applied Loads (σ_1 and σ_2) by Both the Numerical Method and the Analytical Method

σ (MPa)	m		$\dot{k}$ ($\times 10^{-8}\ \mathrm{s}^{-1}$)	h_c
133.2	22.2	Numerical method	5.80	0.26
		Analytical method	4.23	0.25
93.3	16.4	Numerical method	2.0	0.43
		Analytical method	1.30	0.39

plied stress has been established by Chuang:[22]

$$v \propto \sigma_a^m \tag{16}$$

where v is the crack tip velocity and $m = 12$ when the crack growth rate is high. Since $dC/da = C/v$ and $\dot{\epsilon} \propto PC$, a strain rate and applied stress relationship can be obtained after combining Eq. (15) with Eq. (16):

$$\dot{\epsilon} \propto \sigma_a^{m+1} = \sigma_a^{13} \tag{17}$$

which is very close to the values estimated by both the numerical method and the analytical method.

(B) Compression Stress Exponent: The compressive power-law creep exponents given by the numerical method and by the analytical method are 0.8 and 0.9, respectively. From the transmission electron microscopy of postcrept specimens on the compressive side of the flexural creep sample in the paper by Chen and Tien,[21] neither void formation nor dislocation activity was observed. Thus, diffusional creep is the suggested mechanism for the compressive creep. Since the diffusion mechanism corresponds to a power-law creep stress exponent of unity, the estimated and experimental power-law creep exponents agree very well with this deformation mechanism.

The uniaxial compressive tests were carried out at 1170°C at various loads. A typical compressive strain as a function of time plot is shown in Fig. 10. The compressive creep curve shows a very short period of transient creep (less than 10 h) followed by steady-state creep. This short period and high strain of transient creep implies that the residual grain-boundary glassy phase enhances the grain sliding. When the system dilates, limited areas of contact support not only the shear components of the applied stress, but also the normal stress corresponding to a pressure greater than the hydrostatic component of the applied stress. Hence stress concentrations exist at the grain contacts.[5] As the dilatancy diminishes, the steady-state creep is reached.

The results of compressive strain rate as a function of applied stress from the experimental method and by both theoretical estimates are shown in Fig. 11. As can be seen, for a given applied stress, the largest differences between predicted creep rates and experimental data are no more than a factor of 2, which can be regarded as satisfactory in view of the uncertainties involved in the measuring techniques as well as the materials variations. It is evident that the experimental results agree well with the predictions of the numerical and analytical methods. The values for the compressive power-law creep exponent obtained from these three methods are all approximately equal to unity.

(4) Time Dependence of the Stress Distribution

Since the creep parameters estimated by both the numerical and analytical methods were very close, the analytical
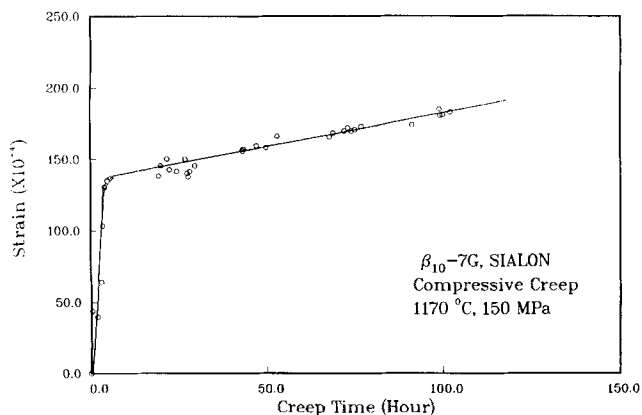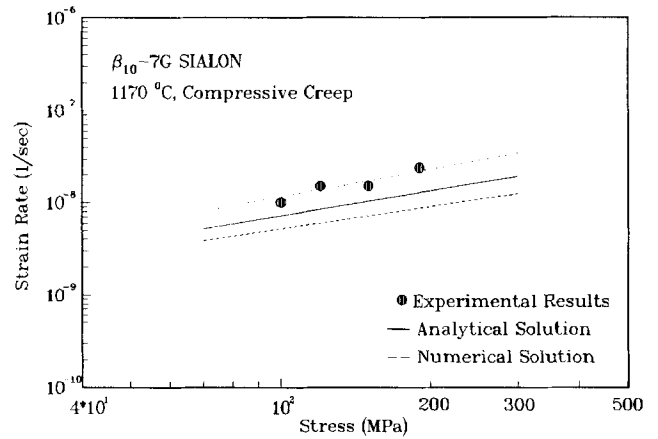

Fig. 11. Theoretical and experimental results of strain rate as a function of stress for compression test at 1170°C.

results will be used to illustrate the time dependence of the stress distribution. Figure 12 shows the stress distribution for an initial elastic stress distribution (curve A) and a drastic relaxation of the stress distribution (curve B) as the creep behavior reaches the steady state. The stress redistribution shows that, because of the relaxation of the tensile stresses, reverse loading occurs in the near midplane region and the damage zone grows toward the compression side of these specimens. The time-dependent stress distribution is believed to stem from (1) load redistribution resulting from development of cracks and cavities on the tensile side of the flexural test specimens and (2) unequal creep rates in tension and compression.

IV. Conclusions

Based on the results and discussions above, the following conclusions can be reached:

(1) Using a numerical method, the uniaxial tensile and compressive power-law creep parameters can be estimated from flexural creep tests. The predicted neutral axis positions agree very well with that determined from indentation flexural creep.

(2) Using the analytical analysis and indentation method, the uniaxial tensile and compressive power-law creep parameters can also be estimated from the flexural creep tests. These results show good agreement with the numerical method.

(3) The power-law creep exponent for compression, $n_c = 1$, further confirms that a diffusional creep mechanism
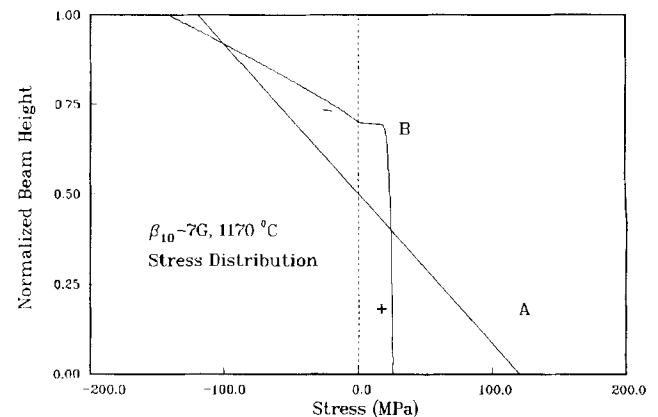

Fig. 10. Typical compressive creep strain as a function of time for sample B60 creep at 1170°C and 150 MPa.

Fig. 12. Typical stress relaxation curve for β_{10}-7G sialon material creep at 1170°C and 133 MPa: (A) elastic initial applied stress, (B) stress after steady-state creep.

is in operation. The power-law creep exponent for tension, $n_t = 13$, suggests a high sensitivity of strain rate of stress due to cavitation.

(4) A shift of the neutral strain axis toward the compression side of a bend bar is a futher confirmation of severe damage in the tensile zone.

(5) The power-law creep exponent from the uniaxial compressive test shows good agreement with the numerical and analytical results. The short transient period might be due to the residual glassy phase enhancing the grain sliding. This mechanism can result in the large strain observed during the transient period. The exponent of unity further confirms that diffusional creep is in operation.

(6) Stresses within the flexure specimens change as a function of time beginning with a linear elastic distribution and reaching nonlinear distributions after steady state is achieved.

References

[1] W. R. Cannon and T. G. Langdon, "Review, Creep of Ceramics: Part 1, Mechanical Characteristics," *J. Mater. Sci.*, **18**, 1–50 (1983).

[2] G.W. Hollenberg, G. R. Terwilliger, and R.S. Gordon, "Calculation of Stresses and Strains in Four-Point Bending Creep Tests," *J. Am. Ceram. Soc.*, **54** [4] 196–99 (1971).

[3] N. J. Tighe and S. M. Wiederhorn, "Effect of Oxidation on the Reliability of Silicon Nitride"; pp. 403–24 in Fracture Mechanics of Ceramics 5. Edited by R. C. Bradt, D. P. H. Hasselman, and F. F. Lange. Plenum Press, New York, 1983.

[4] M. Thouless and A. G. Evans, "Nucleation of Cavities During Creep of Liquid-Phase-Sintered Materials," *J. Am. Ceram. Soc.*, **67** [11] 721–27 (1984).

[5] J. S. Perrin, A. H. Clauer, and B. A. Wilox, "Review of Out-of-Pile and In-Pile Creep of Ceramic Nuclear Fuels," *React. Technol.*, **14**, 99 (1971).

[6] N. J. Tighe, "The Structure of Slow Crack Interfaces in Silicon Nitride," *J. Mater. Sci.*, **13**, 1455–63 (1978).

[7] J. E. Marion, A. G. Evans, M. D. Drory, and D. R. Clarke, "High Temperature Failure Initiation in Liquid Phase," *Acta Metall.*, **31** [10] 1445–57 (1983).

[8] T.-J. Chuang and S. M. Wiederhorn, "Damage-Enhanced Creep in a Sili-

conized Silicon Carbide: Mechanics of Deformation," *J. Am. Ceram. Soc.*, **71** [7] 595–601 (1988).

[9] C.-F. Chen and T.-Y. Tien, "High Temperature Mechanical Properties of SiAlON Ceramics: Microstructural Effects," *Ceram. Sci. Eng. Proc.*, **8** [7–8] 778–95 (1987).

[10] R. Morrell and K. H. G. Ashbee, "High Temperature Creep of Lithium Zinc Silicate Glass-Ceramics," *J. Mater. Sci.*, **8**, 1253–70 (1973).

[11] M. S. Seltzer, "High Temperature Creep of Silicon Based Compounds," *Am. Ceram. Soc. Bull.*, **56** [4] 418–23 (1977).

[12] P. K. Talty and R. A. Dirks, "Determination of Tensile and Compressive Creep Behavior of Ceramic Materials from Bend Tests," *J. Mater. Sci.*, **13**, 580–86 (1978).

[13] A. R. Rosenfield, D. K. Shetty, and W. H. Duckworth, "Estimating Damage Laws from Bend-Test Data," *J. Mater. Sci.*, **20** [1] 935–40 (1985).

[14] A. R. Rosenfield, W. H. Duckworth, and D. K. Shetty, "Damage Analysis of Creep in Bending," *J. Am. Ceram. Soc.*, **68** [9] 483–85 (1985).

[15] A. R. Rosenfield, D. K. Shetty, and W. H. Duckworth, "Estimating Tensile Creep Data from Flexural Data," *J. Am. Ceram. Soc.*, **69** [5] C-108–C-109 (1986).

[16] T.-J. Chuang, "Estimation of Power-Law Creep Parameters from Bend Test Data," *J. Mater. Sci.*, **21**, 165–75 (1986).

[17] C. F. Chen, "Creep Behavior of Sialon and Siliconized SiC"; Ph.D. Thesis. University of Michigan, Ann Arbor, MI, 1987.

[18] S. M. Wiederhorn, L. Chuck, E. R. Fuller, Jr., and N. J. Tighe, "Creep Rupture of Siliconized Silicon Carbide"; pp. 755–73 in Materials Science Research, Vol. 20, Tailoring Multiphase and Composite Ceramics. Edited by R. E. Tressler, G. L. Messing, C. G. Pantano, and R. E. Newham. Plenum Press, New York, 1986.

[19] C.-F. Chen and T.-J. Chuang, "High Temperature Mechanical Properties of SiAlON Ceramics: Creep Characterization," *Ceram. Sci. Eng. Proc.*, **8** [7–8] 796–804 (1987).

[20] T.-J. Chuang, S. M. Wiederhorn, and C. F. Chen, "Transient Behavior of Structural Ceramics under Flexural Creep"; pp. 957–973 in Proceedings of the Third International Conference on Creep and Fracture of Engineering Materials and Structures. Edited by B. Wilshire and R.W. Evans. Institute of Metals, London, 1987.

[21] C. F. Chen and T.Y. Tien, "Microstructural Effect on Creep of Silicon Nitride Ceramics," *Mater. Sci. Forum*, **47**, 204–14 (1989).

[22] T. J. Chuang, "A Diffusive Crack-Growth Model for Creep Fracture," *J. Am. Ceram. Soc.*, **65** [2] 93–103 (1982).

[23] S. M. Wiederhorn, R. E. Roberts, T. J. Chuang, and L. Chuck, "Damage-Enhanced Creep in a Siliconized Silicon Carbide: Phenomenology," *J. Am. Ceram. Soc.*, **71** [7] 602–608 (1988).

[24] D. F. Carroll, "Creep of Siliconized Silicon Carbide"; Ph.D. Thesis. Pennsylvania State University, University Park, PA, 1987.

[25] R. Raj and M. F. Ashby, "Intergranular Fracture at Elevated Temperature," *Acta Metall.*, **23**, 653–66 (1975).

[26] I.W. Chen and A. S. Argon, "Creep Cavitation in 304 Stainless Steel," *Acta Metall.*, **29**, 1321–33 (1981). □